KeAi
CHINESE ROOTS
GLOBAL IMPACT

Available online at www.sciencedirect.com

ScienceDirect

Green Energy & Environment 7 (2022) 449–456

www.keaipublishing.com/gee

Research paper

Mechanistic aspects of facet-dependent CH_4/C_{2+} selectivity over a χ-Fe_5C_2 Fischer–Tropsch catalyst

Thanh Hai Pham [a,b,1], Junbo Cao [a,1], Nan Song [a], Yueqiang Cao [a,*], Bingxu Chen [a], Gang Qian [a], Xinggui Zhou [a], De Chen [c], Xuezhi Duan [a,*]

[a] State Key Laboratory of Chemical Engineering, East China University of Science and Technology, 130 Meilong Road, Shanghai, 200237, China
[b] Vietnam Institute for Tropical Technology and Environmental Protection, 57A Truong Quoc Dung, Ho Chi Minh, Viet Nam
[c] Department of Chemical Engineering, Norwegian University of Science and Technology, N-7491, Trondheim, Norway

Received 29 June 2020; revised 11 October 2020; accepted 13 October 2020
Available online 17 October 2020

Abstract

Structure–performance relationship is a complex issue in iron-catalyzed Fischer–Tropsch synthesis, and it is not easy to elucidate it by experimental investigations. First-principle calculation is a powerful method for explaining experimental results and guiding catalyst design. In this study, we investigated the reaction mechanisms of CH_4 formation and C–C coupling on four χ-Fe_5C_2 surfaces and established the kinetic equations to compare the rates of CH_4 formation and C_1+C_1 coupling reactions and determine the CH_4/C_{2+} selectivity. The results show that the geometry of the χ-Fe_5C_2 surfaces has little effect on the formation rate of CH_4; however, the C_1+C_1 coupling reactions are significantly affected by the surface geometry. The C_1+C_1 coupling reaction rates on the terraced-like (510) and (021) surfaces are much higher than those on the stepped-like (001) and (100) surfaces. Based on these results, we established a Brønsted–Evans–Polanyi (BEP) relationship between the effective barrier difference for CH_4 formation and C_1+C_1 coupling (ΔE_{eff}) and the adsorption energy of C+4H (ΔE_{C+4H}) on χ-Fe_5C_2 surfaces. ΔE_{C+4H} can be used as a descriptor for CH_4/C_{2+} selectivity on different surfaces of χ-Fe_5C_2.

Keywords: Fischer–Tropsch synthesis; χ-Fe_5C_2; Structural sensitivity; CH_4 selectivity

1. Introduction

The Fischer–Tropsch synthesis (FTS) is a complex heterogeneous catalytic reaction. Its reactivity (comprising activity and selectivity) has a strong correlation with the size of the catalyst active phase, and is thus a typical structure-sensitive reaction [1,2]. At present, there are many studies on the size effect of Co and Ru-based FTS catalysts [3–6], and some reliable conclusions have been obtained. Because the conventional Fe-based catalysts used in the past are unsupported, their particle size is relatively large, and the size effect is therefore not significant. However, some recent studies have reported the size effect on Fe-based FTS catalysts. Park et al. [7] studied the size effect of δ-Al_2O_3-supported Fe catalysts, and found that as the particle size and turnover frequency (TOF) increased while the selectivity of CH_4 decreased. Mabaso et al. [8] reported the effect of the particle size of a carbon-supported Fe catalyst, and observed that particles with a size smaller than 7–9 nm displayed significantly lower activity, higher methane selectivity, and lower chain growth probability. Galvis et al. [9] reported the particle size effect of CNF-loaded Fe catalysts, and observed that a decrease from 7 to 2 nm in particle size for catalysts promoted by Na and S results in a 2-fold increase in the apparent TOF based on the initial activity. Furthermore, steady state isotopic transient

* Corresponding authors.
E-mail addresses: yqcao@ecust.edu.cn (Y. Cao), xzduan@ecust.edu.cn (X. Duan).
[1] The authors contributed equally to this work.

https://doi.org/10.1016/j.gee.2020.10.015

kinetic analysis (SSIKTA) revealed that the H coverage is lower for the larger particles and is suppressed upon adding the Na and S promoters, which is in consistent with the observed lower methane selectivity and higher olefin selectivity [10].

It has been found experimentally that iron carbide is the active phase for FT reactions on Fe-based catalysts [11,12], but it is quite difficult to obtain an accurate estimate of the trend in particle size effects under the experimental conditions. With the rapid development of computational chemistry, the use of density functional theory (DFT) calculations to study the reactions on the catalyst surface has become a powerful research method. There have been many good examples where experiments have been combined with simulations to study the structure–efficiency relationship of the catalysts, such as the B5 and C7 site concepts [13–17] on ammonia synthesis catalysts, and the BEP relationship between the activation energy and the reaction energy [18,19]. However, the FTS system is relatively complex, and contains several types of elementary reactions, including C–O bond breaking and C–H and C–C bond formation. There are many reports on the effect of catalyst surface structure on the C–O bond breaking, which has high structural sensitivity [1,2]. However, the possibility of structural effects on C–H and C–C bond formation, reactions that are considered to have low structural sensitivity, is still a matter of considerable debate. Further research is needed on the structure–efficiency relationship of FTS catalysts. Furthermore, it has been proved that iron carbides, especially Hägg iron carbide (χ-Fe_5C_2), are the active phases among the various iron species involved in the complex phase transformation of Fe-based FTS catalysts [11,12,20–22]. Therefore, probing the FTS mechanism and reactivity on the χ-Fe_5C_2 surfaces is highly desirable.

In this work, we have investigated the CH_4 formation and C_1+C_1 coupling reaction mechanisms on four χ-Fe_5C_2 surfaces. The kinetic rate equations were established to compare the rates of CH_4 formation and C_1+C_1 coupling reactions as well as to determine the CH_4/C_{2+} selectivity. Subsequently, we present a descriptor applicable to describe the CH_4/C_{2+} selectivity on χ-Fe_5C_2 surfaces. Finally, the effect of surface structure was associated with a particle size effect on the FTS selectivity. This result might guide the design of highly selective Fe-based FTS catalysts.

2. Computational details

2.1. Methods

The VASP program was used for the DFT calculations in this work, with a GGA-PBE exchange-correlation functional and PAW pseudopotential [23–29]. The cutoff energy for the plane-wave basis set was chosen as 400 eV with a Monkhorst–Pack k points mesh grid and a 0.2 eV energy smearing via the Methfessel-Paxton method [30,31]. The Dimer method [32] was selected to search the transition states (TSs) of the elementary steps in the CH_4 formation and C_1+C_1 coupling reactions. The geometric optimization was performed via the conjugated-gradient method with a force tolerance of 0.03 eV $Å^{-1}$, and the electronic optimization was converged to within 1×10^{-5} eV $atom^{-1}$ [33]. Furthermore, the vibrational frequencies were analyzed to identify the energy minima and TSs by counting the number of imaginary frequencies. The adsorption energies (E_{ads}) was given by $E_{ads} = E_{adsorbate/slab} - E_{adsorbate} - E_{slab}$, where $E_{adsorbate/slab}$, $E_{adsorbate}$ and E_{slab} are the energies of adsorbate bound on the slab, free adsorbate and clean slab, respectively. The activation energy (E_a) of elementary reaction step was calculated by $E_a = E_{TS} - E_{IS}$, where E_{TS} and E_{IS} are the energy of the transition state and the initial state of the reaction step, respectively. Bader analysis [34] was used to evaluate the electronic interaction between iron and carbon atoms. The *d*-band center of these surfaces was given by the following equation [35]:

$$\varepsilon_d = \frac{\int_{-\infty}^{\infty} n(\varepsilon)\varepsilon \, d\varepsilon}{\int_{-\infty}^{\infty} n(\varepsilon) \, d\varepsilon}$$

where $n(\varepsilon)$ is the density of states projected on the d-states. To get the accurate results, the criterion for the electronic optimization was set to be 1×10^{-7} eV $atom^{-1}$.

2.2. χ-Fe_5C_2 surface models

Based on the equilibrium shape of χ-Fe_5C_2 obtained by Wulff construction in our previous study [36,37], four typical thermodynamically stable surfaces, χ-Fe_5C_2 (510)-0.00, χ-Fe_5C_2 (021)-0.00, χ-Fe_5C_2 (001)-0.00 and χ-Fe_5C_2 (100)-0.25, were selected to investigate surface reactions of CH_4 formation and C_1+C_1 coupling. The latter values, such as 0.00, represent the fractional position of the top of the new surface relative to the origin. The χ-Fe_5C_2 (510)-0.00 surface and χ-Fe_5C_2 (021)-0.00 surface were modeled by a p (1×1) slab with four-layered iron and eight-layered carbon. The χ-Fe_5C_2 (001)-0.00 surface was modeled by a p (1×2) supercell slab composed of eight-layered iron and four-layered carbon. For the χ-Fe_5C_2 (100)-0.25 surface, a p (2×1) supercell slab with six-layered iron and two-layered carbon was used. For the (510) and (021) surfaces, the bottom two-layered iron and four-layered carbon were fixed, with the top two-layered iron, four-layered carbon and adsorbates relaxed. For the (001) surface, the bottom four-layered iron and two-layered carbon were fixed, while the top four-layered iron, two-layered carbon and adsorbates were relaxed. For the (100) surface, only the top three-layered iron, one-layered carbon and adsorbates were allowed to relax. The k point meshes of ($4 \times 2 \times 1$), ($3 \times 2 \times 1$), ($3 \times 2 \times 1$) and ($2 \times 4 \times 1$) were used for (510), (021), (001) and (100) surfaces, respectively. The vacuum spacing was approximately 10 Å. The top and side views of the χ-Fe_5C_2 surfaces studied are illustrated in Fig. 1. The supercell sizes, relaxed layers, k point grids, and vacuum space of the four χ-Fe_5C_2 surfaces have been tested and proved to be reasonable in previous studies [36,37].

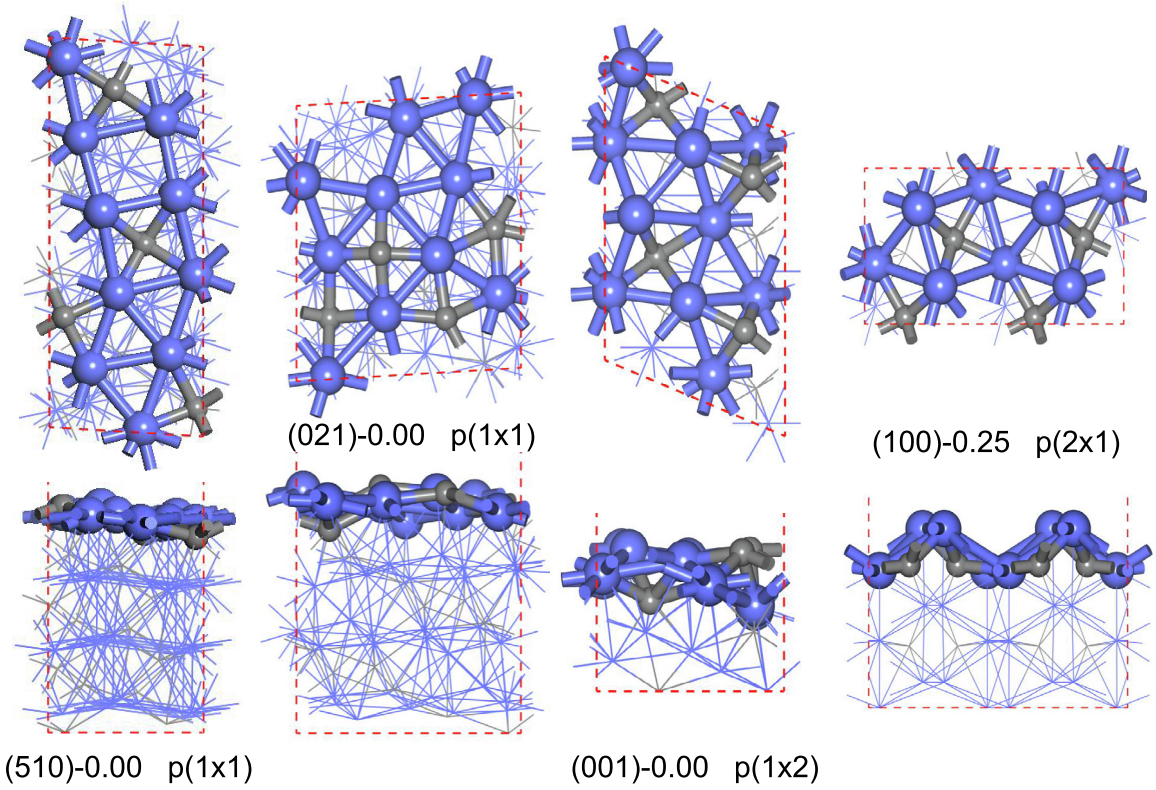

Fig. 1. Top (top) and side (bottom) views of χ-Fe_5C_2 surfaces (Blue: Fe atoms; gray: C atoms).

3. Results and discussion

3.1. CH_x hydrogenation

First, we studied the CH_x (x = 0–3) hydrogenation reactions on the four χ-Fe_5C_2 surfaces. The adsorption energies of H and CH_x on the four surfaces are shown in Table S1. The energy barriers and reaction energies of four elementary reactions are shown in Table 1. The optimized structures of the chemisorbed C_1 species and TSs of the elementary steps are shown in Figs. S1-S2. In addition, Fig. 2 illustrates the energy profile of CH_4 formation on four χ-Fe_5C_2 surfaces.

As shown in Table 1, the barriers of each step on the four surfaces are close (except R3 and R4 on the (100) surface), but there are obvious variations in the reaction energies. The hydrogenation reaction energies on the terraced-like (510) and (021) surfaces are much higher than those on the stepped-like (001) and (100) surfaces (except R4 of the (100) surface). This indicates that the barrier is only slightly affected by the structure, whereas the reaction energy (the adsorption energy of CH_x + H) is strongly affected. The variation of C+4H, CH+3H, CH_2+3H, and CH_3+H adsorption energies on the four surfaces are 1.25, 0.92, 0.47 and 0.65 eV, respectively (Fig. 2). Table S1 shows that there are significant differences among the CH_x adsorption energies (especially between C and CH) on the four surfces, while the adsorption energies of H are closer (0.61–0.72 eV). The adsorption energies of C and CH on the (510) and (021) surfaces are significantly smaller than those on the (001) and (100) surfaces. This can be explained by the difference in adsorption positions. The adsorption sites of C and CH on the (510) and (021) surfaces are 4-fold sites, whereas they are 3-fold sites on the (001) and (100) surfaces (Fig. S1).

To calculate the CH_x coverage (θ_{CHx}) and CH_4 formation rate on the different surfaces, we introduce the following two assumptions:

(1) **CH_x can reach equilibrium on the different surfaces.** CH_2 and CH_3 diffuse very readily [38] while C and CH diffuse with difficulty. However, CH_x dissociation on the

Table 1
The barriers and reaction energies of CH_x hydrogenation on the χ-Fe_5C_2 surfaces.

Reaction		E_a (eV)				ΔE_r (eV)			
		(510)	(021)	(001)	(100)	(510)	(021)	(001)	(100)
R1	C + H→CH	0.93	0.77	0.91	0.93	0.18	0.28	−0.16	−0.17
R2	CH + H→CH_2	0.87	0.67	0.66	0.60	0.85	0.74	0.40	0.30
R3	CH_2+H→CH_3	0.79	0.69	0.72	0.35	0.31	0.29	0.07	−0.16
R4	CH_3+H→CH_4	0.84	0.79	0.72	1.07	0.38	0.27	0.15	0.80

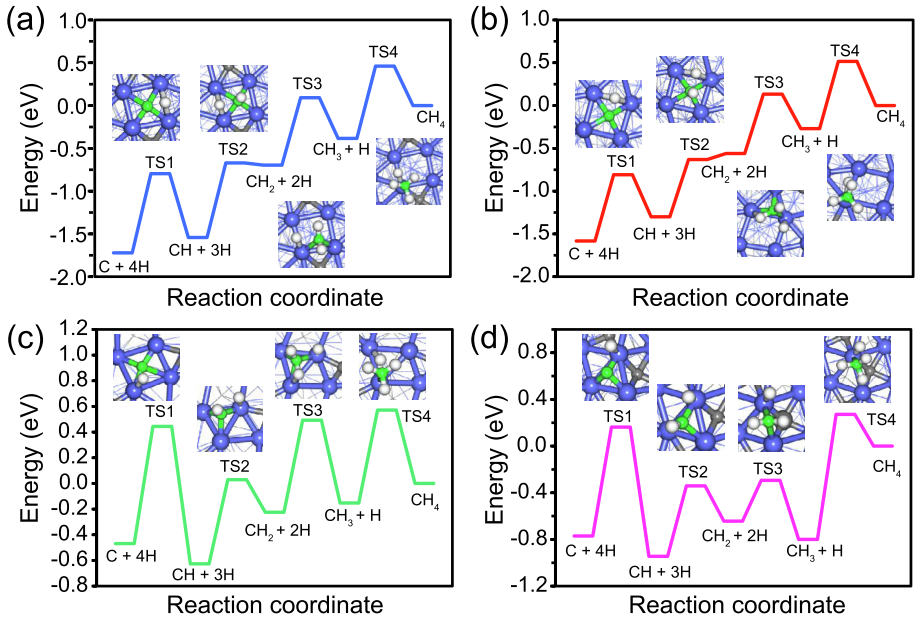

Fig. 2. Energy profiles of CH_4 formation from C+4H on (a) χ-Fe_5C_2 (510), (b) χ-Fe_5C_2 (021), (c) χ-Fe_5C_2 (001) and (d) χ-Fe_5C_2 (100) surfaces. The transition-state configurations of the four stepwise hydrogenations are shown in the insets.

surface of χ-Fe_5C_2 is very easy; thus, C and CH can be formed by diffusion and dissociation of CH_2 and CH_3.

(2) **R4 is the rate-determining step of C hydrogenation.** Since the coverage of CH_3 is the smallest and the energy barrier of R4 is large, it can be assumed that the three preceding hydrogenation steps can reach equilibrium.

These two assumptions have been used in previous studies [20,21,39,40], which also investigated the reaction mechanisms of CH_4 formation and C_1+C_1 coupling on different catalyst surfaces. Using these two assumptions, we can get an expression for CH_x coverage as follows (The derivation details are given in Supporting Information):

$$\theta_{CH_i}^{(S)} = e^{-\left(E_i^{(S)}/RT\right)}\theta_C^{(510)} t_{(S)}^{i} \frac{\theta_*^{(S)}}{\theta_*^{(510)}} \tag{1}$$

where $\theta_{CH_i}^{(S)}$ is the coverage of CH_i (i = 0–3) on the (S) surface; $E_i^{(S)}$ is the energy difference between CH_i on the (S) surface and C+iH on the (510) surface (this value is shown in Fig. 2); $\theta_C^{(510)}$ is the coverage of C on the (510) surface; t is θ_H/θ_* of the (S) surface; and $\theta_*^{(S)}$ and $\theta_*^{(510)}$ are the coverages of the free sites on the (S) and (510) surfaces, respectively.

The CH_4 formation rate expression is (The derivation details are in Supporting Information):

$$\begin{aligned} r_{CH_4}^{(S)} &= Ae^{-\left(E_3^{(S)}+E_{a,R_4}^{(S)}\right)\Big/RT}\theta_C^{(510)}\theta_H^{(S)}t_{(S)}^{3}\frac{\theta_*^{(S)}}{\theta_*^{(510)}} \\ &= Ae^{-E_{eff,CH_4}^{(S)}\Big/RT}\theta_C^{(510)}\theta_H^{(S)}t_{(S)}^{3}\frac{\theta_*^{(S)}}{\theta_*^{(510)}} \end{aligned} \tag{2}$$

where A is the pre-exponental factor, assumed to be constant for the surface reactions [21,39,40]; $E_{a,R_4}^{(S)}$ is energy barrier of R_4 on the (S) surface; $\theta_H^{(S)}$ is the coverage of H on the (S) surface; and $E_{eff,CH_4}^{(S)} = E_3^{(S)} + E_{a,R_4}^{(S)}$ is defined as the effective barrier of CH_4 formation on the (S) surface.

The effects of $\theta_H^{(S)}$, t, and the $\frac{\theta_*^{(S)}}{\theta_*^{(510)}}$ value are much smaller than that of $E_{\mathrm{eff},CH_4}^{(S)}$. Therefore, we analyzed the CH_4 generation rate on different surfaces by comparing the values of $E_{\mathrm{eff},CH_4}^{(S)}$. As can be seen from Fig. 2, the values of E_{eff,CH_4} on the (510) (021) (001), and (100) surfaces were 2.18, 2.24, 2.29, and 1.99 eV, respectively, with a small variation range of 0.30 eV. It can be inferred that the structures of χ-Fe_5C_2 surfaces have little effect on CH_4 formation.

3.2. C_1+C_1 coupling

We calculated nine possible CH_x + CH_y coupling reactions on the four χ-Fe_5C_2 surfaces. The barriers and reaction energies are summarized in Table 2, and the transition-state structures are shown in Fig. S2.

The rate expression for the C_1+C_1 coupling reaction is:

$$\begin{aligned} r_{CH_i+CH_j}^{(S)} &= Ae^{-E_{a,i+j}^{(S)}/RT}\theta_{CH_i}^{(S)}\theta_{CH_j}^{(S)} \\ &= Ae^{-\left(E_{a,i+j}^{(S)}+E_i^{(S)}+E_j^{(S)}\right)/RT}t_{(S)}^{i+j}\left(\theta_C^{(510)}\frac{\theta_*^{(S)}}{\theta_*^{(510)}}\right)^2 \\ &= Ae^{-E_{eff,i+j}^{(S)}/RT}t_{(S)}^{i+j}\left(\theta_C^{(510)}\frac{\theta_*^{(S)}}{\theta_*^{(510)}}\right)^2 \end{aligned} \tag{3}$$

where $E_{eff,i+j}^{(S)} = E_{a,i+j}^{(S)} + E_i^{(S)} + E_j^{(S)}$ is defined as the effective barrier of the CH_i + CH_j reaction. It is noteworthy that the C_1+C_1 coupling reaction rate changes exponentially with $E_{eff,i+j}^{(S)}$. We therefore took the effective barrier here as a descriptor to estimate the C_1+C_1 coupling reaction rate. Fig. 3

Table 2
The barriers and reaction energies of $CH_x + CH_y$ coupling on the χ-Fe_5C_2 surfaces.

Reaction		E_a (eV)				ΔE_r (eV)			
		(510)	(021)	(001)	(100)	(510)	(021)	(001)	(100)
R5	C + C	1.59	1.91	1.18	1.45	1.23	1.21	−0.39	−0.71
R6	C + CH	1.09	1.38	0.78	1.02	0.65	0.85	−0.22	−0.72
R7	$C + CH_2$	1.09	1.31	0.89	1.09	0.15	0.62	−0.41	−0.78
R8	$C + CH_3$	1.21	0.76	0.90	1.42	−0.07	−0.16	−0.36	−0.23
R9	CH + CH	0.96	1.27	0.94	1.45	0.43	0.91	0.42	−0.13
R10	$CH + CH_2$	1.03	1.63	1.10	1.58	0.64	0.72	0.52	−0.11
R11	$CH + CH_3$	1.52	1.19	1.52	1.79	0.42	0.45	0.64	0.44
R12	$CH_2 + CH_2$	0.98	1.17	0.60	0.30	−0.02	0.16	−0.17	−0.69
R13	$CH_2 + CH_3$	1.45	0.87	1.47	1.28	0.23	−0.06	0.11	0.14

compares $E_i^{(S)} + E_j^{(S)}$, $E_{a,i+j}^{(S)}$, and $E_{eff,i+j}^{(S)}$ on the four χ-Fe_5C_2 surfaces.

It can be seen that on the (510) (021) and (001) surfaces, the C + CH and CH + CH reactions are the main C_1+C_1 coupling pathways, owing to their having the lowest effective barriers, while on the (100) surface, CH_2+CH_2 is the main C_1+C_1 coupling pathway. Since the reaction rate of the main coupling pathway is several orders larger than that of the others, the C_1+C_1 coupling rate on the surface will be approximately equal to the rate of the main coupling reaction. Thus:

$$r_{C_1+C_1}^{(S)} \approx max\left\{r_{CH_i+CH_j}^{(S)}\right\} = Ae^{-min\left\{E_{eff,i+j}^{(S)}\right\}/RT} t_{(S)}^{i+j}\left(\theta_C^{(510)}\frac{\theta_*^{(S)}}{\theta_*^{(510)}}\right)^2$$
$$= Ae^{-E_{eff,C_1+C_1}^{(S)}/RT} t_{(S)}^{i+j}\left(\theta_C^{(510)}\frac{\theta_*^{(S)}}{\theta_*^{(510)}}\right)^2 \quad (4)$$

Here we can use $E_{eff,C_1+C_1}^{(S)} = min\{E_{eff,i+j}^{(S)}\}$ to compare the C_1+C_1 coupling rates on the different surfaces. As can be seen from Fig. 3, $E_{eff,C_1+C_1}^{(S)}$ (red values) increases in the order (510) < (021) < (100) < (001), hence, the C_1+C_1 coupling rate decreases in the order (510) > (021) > (100) > (001). The variation of $E_{eff,C_1+C_1}^{(S)}$ on the four χ-Fe_5C_2 surfaces is very large (1.86 eV). Therefore, it can be inferred that the structures of the χ-Fe_5C_2 surfaces can have a significant effect on the C_1+C_1 coupling reaction rate.

3.3. CH_4/C_{2+} selectivity

To compare the CH_4/C_{2+} selectivity on the four χ-Fe_5C_2 surfaces, we calculated the ratio of the rate of CH_4 formation to that of C_1+C_1 coupling [38,41,42], as shown in Eq. (5).

$$\frac{r_{CH_4}^{(S)}}{r_{C_1+C_1}^{(S)}} = Ae^{-\left(E_{eff,CH_4}^{(S)} - E_{eff,C_1+C_1}^{(S)}\right)/RT} t_{(S)}^{3-(i+j)}\frac{\theta_H^{(S)}\theta_*^{(510)}}{\theta_C^{(510)}\theta_*^{(S)}}$$
$$= Ae^{-\Delta E_{eff}^{(S)}/RT} t_{(S)}^{4-(i+j)}\frac{\theta_*^{(510)}}{\theta_C^{(510)}} \quad (5)$$

where $\Delta E_{eff}^{(S)} = E_{eff,CH_4}^{(S)} - E_{eff,C_1+C_1}^{(S)}$ is the effective barrier difference between CH_4 formation and C_1+C_1 coupling on the (S) surface. The surface with a larger $\Delta E_{eff}^{(S)}$ may have a smaller CH_4/C_{2+} selectivity. We summarize the effective barriers and effective barrier differences between CH_4 formation and C_1+C_1 coupling on the four χ-Fe_5C_2 surfaces in Table 3. It can be seen that $\Delta E_{eff}^{(S)}$ decreases in the order (510) > (021) > (100) > (001). Hence, the CH_4/C_{2+} selectivity increases in the order (510) < (021) < (100) < (001),

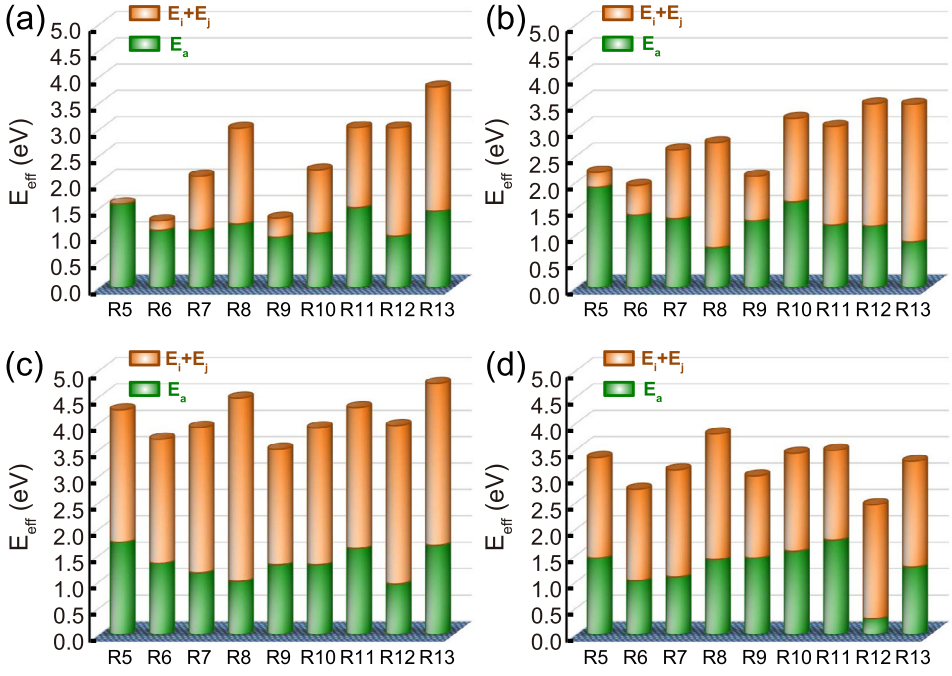

Fig. 3. The energy barriers, relative energy of reactants and effective barriers of $CH_i + CH_j$ coupling on (a) χ-Fe_5C_2 (510), (b) χ-Fe_5C_2 (021), (c) χ-Fe_5C_2 (001) and (d) χ-Fe_5C_2 (100) surfaces.

Table 3
The values of E_{eff,CH_4}, E_{eff,C_1+C_1}, ΔE_{eff}, and the C+4H adsorption energy (ΔE_{C+4H}, with respect to gaseous CH_4) on the χ-Fe_5C_2 surfaces.

	(510)	(021)	(001)	(100)-0.25
E_{eff,CH_4} (eV)	2.18	2.24	2.29	1.99
E_{eff,C_1+C_1} (eV)	1.27	1.94	3.13	2.46
ΔE_{eff} (eV)	0.91	0.30	−0.83	−0.46
ΔE_{C+4H} (eV)	−1.72	−1.58	−0.47	−0.77

indicating that the structures of the χ-Fe_5C_2 surfaces have a significant effect on CH_4/C_{2+} selectivity.

Furthermore, we correlated E_{eff,CH_4}, E_{eff,C_1+C_1}, and ΔE_{eff} with the adsorption energy of C+4H (ΔE_{C+4H}, relative to the gas phase CH_4) on the four χ-Fe_5C_2 surfaces. As seen in Fig. 4a, there is a linear relationship between E_{eff,C_1+C_1} and ΔE_{C+4H}, with E_{eff,C_1+C_1} increasing as ΔE_{C+4H} decreases in magnitude. However, E_{eff,CH_4} is insensitive to ΔE_{C+4H}. More importantly, there is also a strong linear relationship between ΔE_{eff} and ΔE_{C+4H}, which implies that the CH_4 selectivity on a particular surface of χ-Fe_5C_2 can be measured by ΔE_{C+4H}. According to our results, the terraced-like surfaces of the χ-Fe_5C_2 catalyst have a higher C_1+C_1 coupling activity, resulting in a lower CH_4 selectivity. This means that larger catalyst particles with a larger percentage of terraced-like surfaces should have lower CH_4 selectivity, which is in good agreement with the experimental results [7,9]. Notably, these four surfaces exhibit different geometric structures together with different electronic properties, which may contribute to a trade-off for the CH_4 formation and C_1+C_1 coupling. To figure out the dominant factor, the *d*-band center and charge analysis are further calculated for these four surfaces and correlated with the effective barriers for CH_4 formation and C_1+C_1 coupling. As shown in Fig. 4b–d, the values of E_{eff,CH_4}, E_{eff,C_1+C_1}, and ΔE_{eff} are also well correlated with the *d*-band center of the surfaces. Similarly, E_{eff,CH_4} is independent of the *d*-band center, indicating that the formation of CH_4 is insensitive to the geometry of the surfaces. In contrast, E_{eff,C_1+C_1} shows a linear relationship with the *d*-band center, that is, the coupling process clearly depends on the surface geometry. As a result, ΔE_{eff} shows a positive linear relationship with the *d*-band center, which is in accordance with the trend against ΔE_{C+4H}, based on *d*-band theory [43]. ΔE_{eff} is further correlated with the charge of the iron atoms on the surfaces. As shown in Fig. 4e, ΔE_{eff} show a "reverse volcano" trend with the atomic charge of the surface iron atoms, which is different from the linear trend seen with CO activation [44]. Thus, the atomic charge of iron should be optimized for the targeted FTS catalysts in accordance with the trade-off between CO activation and CH_4/C_{2+} selectivity.

3.4. Additional discussion

Cheng et al. [40] found that on stepped surfaces with similar B5 active sites of different metals, the CH_4 formation rates change significantly, whereas the C_1+C_1 coupling rates are relatively close. In their study, the electronic structure of the particular metal is the main influencing factor. In contrast, our results focus on different surfaces of the same iron carbide with very similar electronic structures, so that the geometry of the particular surface becomes the main influencing factor. Fig. 4 shows that the CH_4 formation rates did not change much, whereas the variation in C_1+C_1 coupling rates is very

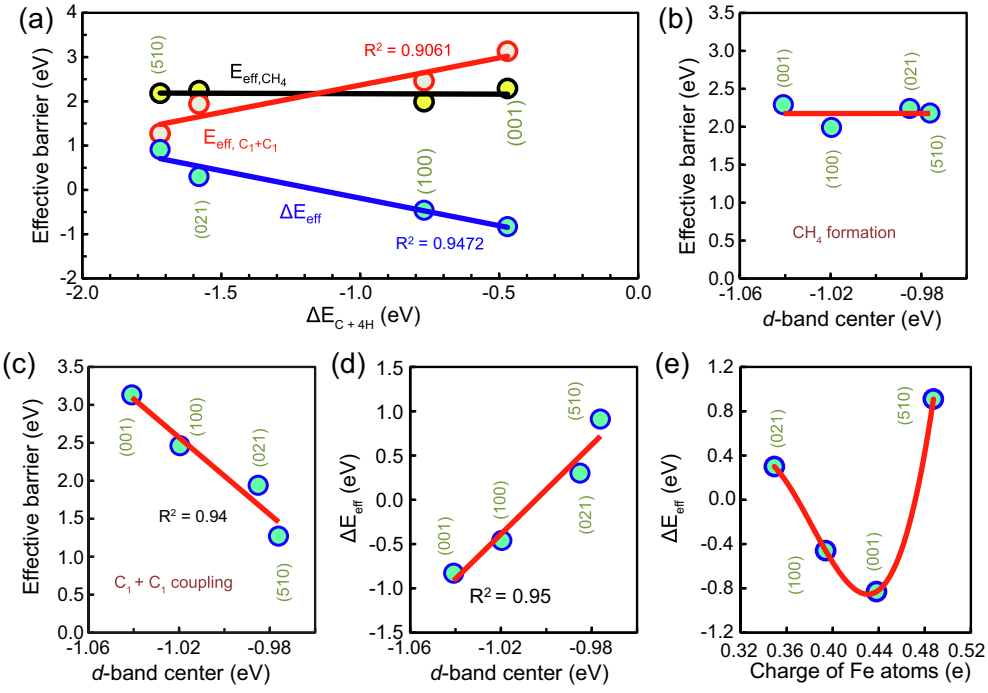

Fig. 4. (a) Plots of E_{eff,CH_4}, E_{eff,C_1+C_1}, and ΔE_{eff} as functions of ΔE_{C+4H} on χ-Fe_5C_2 (510), χ-Fe_5C_2 (021), χ-Fe_5C_2 (001) and χ-Fe_5C_2 (100) surfaces; (b), (c), and (d) plots of E_{eff,CH_4}, E_{eff,C_1+C_1}, and ΔE_{eff}, respectively, as functions of the *d*-band center of the χ-Fe_5C_2 surfaces; (e) plot of ΔE_{eff} as a function of the amount of charge on Fe atoms on the χ-Fe_5C_2 surfaces.

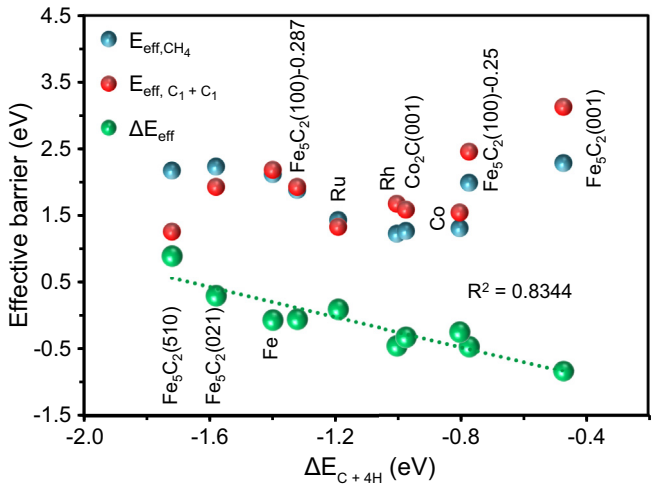

Fig. 5. Plots of E_{eff,CH_4}, E_{eff,C_1+C_1}, and ΔE_{eff} as functions of ΔE_{C+4H} on χ-Fe_5C_2, Co_2C, Fe, Ru, Co, and Rh surfaces.

marked. Combining our work with the study by Cheng et al. [40], it can be inferred that the electronic structure may be the main factor affecting the rate of CH_4 formation, while the geometry may strongly influence the rate of C_1+C_1 coupling. The selectivity of CH_4/C_{2+} is determined by the combination of electronic and geometric structure. Fig. 5 includes the results of both this work and the work of Cheng et al. [21,40]. It can be seen that ΔE_{C+4H} can be used as a descriptor for CH_4/C_{2+} selectivity on the multi-surfaces of different catalysts. This conclusion provides a convenient screening method for the rational design of the catalysts.

4. Conclusions

This work presents a systematic investigation by DFT of the surface-structure dependence of CH_4/C_{2+} selectivity in χ-Fe_5C_2-catalyzed FTS. The effect of the geometry of the χ-Fe_5C_2 surfaces on the formation rate of CH_4 is not significant; however, the C_1+C_1 coupling reactions are significantly affected by the surface geometry. The C_1+C_1 coupling reaction rates on terraced-like (510) and (021) surfaces are much higher than the rates on stepped-like (001) and (100) surfaces. The terraced-like surfaces of the χ- Fe_5C_2 catalyst have higher C_1+C_1 coupling activity, resulting in lower CH_4 selectivity. This means that larger catalyst particles may have lower CH_4 selectivity. Combining this with the reported experimental results, we speculate that surface electronic structure is the main factor affecting the formation of CH_4, surface geometric structure is the main factor affecting C_1+C_1 coupling, and that the CH_4/C_{2+} selectivity is affected by both of the above factors. Moreover, the adsorption energy of C+4H (ΔE_{C+4H}) reflects the effects of both the electronic and geometric structures of a surface, and can be used as a good descriptor to estimate the CH_4/C_{2+} selectivity, not only on different surfaces of χ-Fe_5C_2 , but also that of other catalysts. Thus, this result may be of great interest in FTS catalyst design and optimization.

Conflict of interest

The authors declare that the research was conducted in the absence of any commercial or financial relationships that could be construed as a potential conflict of interest.

Acknowledgments

This work was financially supported by the Natural Science Foundation of China (21922803 and 21776077), the Program for the Professor of Special Appointment (Eastern Scholar) at Shanghai Institutions of Higher Learning, the State Key Laboratory of Organic-Inorganic Composites (oic-201801007), and the Open Project of State Key Laboratory of Chemical Engineering (SKLChe-15C03).

Appendix A. Supplementary data

Supplementary data to this article can be found online at https://doi.org/10.1016/j.gee.2020.10.015.

References

[1] R.A. van Santen, Acc. Chem. Res. 42 (2008) 57–66.
[2] M. Boudart, M.A. McDonald, J. Phys. Chem. 88 (1984) 2185–2195.
[3] J.P. den Breejen, P.B. Radstake, G.L. Bezemer, J.H. Bitter, V. Froseth, A. Holmen, K.P. de Jong, J. Am. Chem. Soc. 131 (2009) 7197–7203.
[4] D. Barkhuizen, I. Mabaso, E. Viljoen, C. Welker, M. Claeys, E. van Steen, J.C. Fletcher, Pure Appl. Chem. 78 (2006) 1759–1769.
[5] G.L. Bezemer, J.H. Bitter, H.P.C.E. Kuipers, H. Oosterbeek, J.E. Holewijn, X. Xu, F. Kapteijn, A.J. van Dillen, K.P. de Jong, J. Am. Chem. Soc. 128 (2006) 3956–3964.
[6] E. Iglesia, S.L. Soled, R.A. Fiato, J. Catal. 137 (1992) 212–224.
[7] J.Y. Park, Y.J. Lee, P.K. Khanna, K.W. Jun, J.W. Bae, Y.H. Kim, J. Mol. Catal. Chem. 323 (2010) 84–90.
[8] E.I. Mabaso, E. van Steen, M. Claeys, DGMK Tagungsbericht 4 (2006) 93–100.
[9] H.M. Torres Galvis, J.H. Bitter, T. Davidian, M. Ruitenbeek, A.I. Dugulan, K.P. de Jong, J. Am. Chem. Soc. 134 (2012) 16207–16215.
[10] J. Xie, J. Yang, A.I. Dugulan, A. Holmen, D. Chen, K.P. de Jong, M.J. Louwerse, ACS Catal. 6 (2016) 3147–3157.
[11] E. de Smit, F. Cinquini, A.M. Beale, O.V. Safonova, W. van Beek, P. Sautet, B.M. Weckhuysen, J. Am. Chem. Soc. 132 (2010) 14928–14941.
[12] C. Yang, H. Zhao, Y. Hou, D. Ma, J. Am. Chem. Soc. 38 (2012) 15814–15821.
[13] R. van Hardeveld, A. van Montfoort, Surf. Sci. 4 (1966) 396–430.
[14] K. Honkala, A. Helleman, I.N. Remediakis, A. Logadottir, A. Carlsson, S. Dahl, J. K. Nørskov. Science 307 (2005) 555–558.
[15] M. Lahav, D. Rabinovitch, J.F. Nicoud, G. Balavoine, H. Kagan, G. Tsoucaris, Science 273 (1996) 20.
[16] S. Dahl, A. Logadottir, R.C. Egeberg, J.H. Larsen, I. Chorkendorff, E. Tornqvist, J.K. Norskov, Phys. Rev. Lett. 83 (1999) 1814.
[17] N.D. Spencer, R.C. Schoonmaker, G.A. Somorjai, J. Catal. 74 (1982) 129–135.
[18] B. Hammer, J.K. Norskov, Adv. Catal. 45 (2000) 71–129.
[19] Z.P. Liu, P. Hu, J. Chem. Phys. 115 (2001) 4977–4980.
[20] C.F. Huo, Y.W. Li, J. Wang, H. Jiao, J. Am. Chem. Soc. 131 (2009) 14713–14721.
[21] J. Cheng, P. Hu, P. Ellis, S. French, G. Kelly, C.M. Lok, J. Phys. Chem. C 114 (2009) 1085–1093.
[22] T. Herranz, S. Rojas, F.J. Perez-Alonso, M. Ojeda, P. Terreros, J.L.G. Fierro, J. Catal. 243 (2006) 199–211.

[23] G. Kresse, J. Hafner, Phys. Rev. B 47 (1993) 558–561.
[24] G. Kresse, J. Hafner, Phys. Rev. B 49 (1994) 14251–14269.
[25] G. Kresse, J. Furthmuller, Comput. Mater. Sci. 6 (1996) 15–50.
[26] G. Kresse, J. Furthmuller, Phys. Rev. B 54 (1996) 11169–11186.
[27] P.E. Blochl, Phys. Rev. B 50 (1994) 17953–17979.
[28] G. Kresse, D. Joubert, Phys. Rev. B 59 (1999) 1758–1775.
[29] J.P. Perdew, K. Burkem, M. Ernzerhof, Phys. Rev. Lett. 77 (1996) 3865–3868.
[30] H.J. Monkhorst, J.D. Pack, Phys. Rev. B 13 (1976) 5188–5192.
[31] M. Methfessel, A.T. Paxton, Phys. Rev. B 40 (1989) 3616–3621.
[32] G. Henkelman, H. Jonsson, J. Chem. Phys. 111 (1999) 7010–7022.
[33] D. Sheppard, R. Terrell, G. Henkelman, J. Chem. Phys. 128 (2008) 134106.
[34] T.H. Pham, Y. Qi, Y. Jia, X.Z. Duan, G. Qian, X.G. Zhou, D. Chen, W. Yuan, ACS Catal. 5 (2015) 2203–2208.
[35] W. Tang, E. Sanville, G. Henkelman, J. Phys. Condens. Matter 21 (2009) 084204.
[36] B. Hammer, J.K. Nørskov, Adv. Catal. 45 (2000) 71–129.
[37] T.H. Pham, X.Z. Duan, G. Qian, X.G. Zhou, D. Chen, J. Phys. Chem. C 118 (2014) 10170–10176.
[38] A. Govender, D. Curulla Ferré, J.W. Niemantsverdriet, ChemPhysChem 13 (2012) 1591–1596.
[39] J. Cheng, X.Q. Gong, P. Hu, C.M. Lok, P. Ellis, S. French, J. Catal. 254 (2008) 285–295.
[40] J. Cheng, P. Hu, P. Ellis, S. French, G. Kelly, C.M. Lok, J. Phys. Chem. C 113 (2009) 8858–8863.
[41] D.C. Sorescu, Phys. Rev. B 73 (2006) 155420.
[42] D.B. Cao, Y.W. Li, J. Wang, H. Jiao, J. Phys. Chem. C 112 (2008) 14883–14890.
[43] J.K. Nørskov, F.A. Pedersen, F. Studt, T. Bligaard, Proc. Natl. Acad. Sci. Unit. States Am. 108 (2011) 937–943.
[44] B.X. Chen, D. Wang, X.Z. Duan, W. Liu, Y.F. Li, G. Qian, W.K. Yuan, A. Holmen, X.G. Zhou, D. Chen, ACS Catal. 8 (2018) 2709–2714.